Radboud Repository

Radboud University Nijmegen

PDF hosted at the Radboud Repository of the Radboud University Nijmegen

The following full text is a preprint version which may differ from the publisher's version.

For additional information about this publication click this link.
http://hdl.handle.net/2066/124958

Please be advised that this information was generated on 2021-10-18 and may be subject to change.

EUROPEAN LABORATORY FOR PARTICLE PHYSICS

CERN-PPE/97-121
2 December 1997

Search for a Massive Di-photon Resonance at $\sqrt{s} = 91 - 172$ GeV

The OPAL Collaboration

Abstract

A search for the resonant production of high mass photon pairs associated with a leptonic or hadronic system has been performed using a total data sample of 25.7 pb^{-1} taken at centre-of-mass energies between 130 GeV and 172 GeV with the OPAL detector at LEP. The observed number of events is consistent with the expected number from Standard Model processes. The observed candidates are combined with search results from $\sqrt{s} \approx M_{\mathrm{Z}}$ to place limits on $B(\mathrm{H}^0 \to \gamma\gamma)$ within the Standard Model for Higgs boson masses up to 77 GeV, and on the production cross section of any scalar resonance decaying into di-photons. Upper limits on $B(\mathrm{H}^0 \to \gamma\gamma) \times \sigma(\mathrm{e}^+\mathrm{e}^- \to \mathrm{H}^0\mathrm{Z}^0)$ of 290 – 830 fb are obtained over $40 < M_{\mathrm{H}} < 160$ GeV. Higgs scalars which couple only to gauge bosons at Standard Model strength are ruled out up to a mass of 76.5 GeV at the 95% confidence level.

(Submitted to Zeitschrift für Physik C)

The OPAL Collaboration

K. Ackerstaff[8], G. Alexander[23], J. Allison[16], N. Altekamp[5], K.J. Anderson[9], S. Anderson[12], S. Arcelli[2], S. Asai[24], D. Axen[29], G. Azuelos[18,a], A.H. Ball[17], E. Barberio[8], R.J. Barlow[16], R. Bartoldus[3], J.R. Batley[5], S. Baumann[3], J. Bechtluft[14], C. Beeston[16], T. Behnke[8], A.N. Bell[1], K.W. Bell[20], G. Bella[23], S. Bentvelsen[8], S. Bethke[14], O. Biebel[14], A. Biguzzi[5], S.D. Bird[16], V. Blobel[27], I.J. Bloodworth[1], J.E. Bloomer[1], M. Bobinski[10], P. Bock[11], D. Bonacorsi[2], M. Boutemeur[34], B.T. Bouwens[12], S. Braibant[12], L. Brigliadori[2], R.M. Brown[20], H.J. Burckhart[8], C. Burgard[8], R. Bürgin[10], P. Capiluppi[2], R.K. Carnegie[6], A.A. Carter[13], J.R. Carter[5], C.Y. Chang[17], D.G. Charlton[1,b], D. Chrisman[4], P.E.L. Clarke[15], I. Cohen[23], J.E. Conboy[15], O.C. Cooke[8], M. Cuffiani[2], S. Dado[22], C. Dallapiccola[17], G.M. Dallavalle[2], R. Davis[30], S. De Jong[12], L.A. del Pozo[4], K. Desch[3], B. Dienes[33,d], M.S. Dixit[7], E. do Couto e Silva[12], M. Doucet[18], E. Duchovni[26], G. Duckeck[34], I.P. Duerdoth[16], D. Eatough[16], J.E.G. Edwards[16], P.G. Estabrooks[6], H.G. Evans[9], M. Evans[13], F. Fabbri[2], M. Fanti[2], A.A. Faust[30], F. Fiedler[27], M. Fierro[2], H.M. Fischer[3], I. Fleck[8], R. Folman[26], D.G. Fong[17], M. Foucher[17], A. Fürtjes[8], D.I. Futyan[16], P. Gagnon[7], J.W. Gary[4], J. Gascon[18], S.M. Gascon-Shotkin[17], N.I. Geddes[20], C. Geich-Gimbel[3], T. Geralis[20], G. Giacomelli[2], P. Giacomelli[4], R. Giacomelli[2], V. Gibson[5], W.R. Gibson[13], D.M. Gingrich[30,a], D. Glenzinski[9], J. Goldberg[22], M.J. Goodrick[5], W. Gorn[4], C. Grandi[2], E. Gross[26], J. Grunhaus[23], M. Gruwé[8], C. Hajdu[32], G.G. Hanson[12], M. Hansroul[8], M. Hapke[13], C.K. Hargrove[7], P.A. Hart[9], C. Hartmann[3], M. Hauschild[8], C.M. Hawkes[5], R. Hawkings[27], R.J. Hemingway[6], M. Herndon[17], G. Herten[10], R.D. Heuer[8], M.D. Hildreth[8], J.C. Hill[5], S.J. Hillier[1], P.R. Hobson[25], R.J. Homer[1], A.K. Honma[28,a], D. Horváth[32,c], K.R. Hossain[30], R. Howard[29], P. Hüntemeyer[27], D.E. Hutchcroft[5], P. Igo-Kemenes[11], D.C. Imrie[25], M.R. Ingram[16], K. Ishii[24], A. Jawahery[17], P.W. Jeffreys[20], H. Jeremie[18], M. Jimack[1], A. Joly[18], C.R. Jones[5], G. Jones[16], M. Jones[6], U. Jost[11], P. Jovanovic[1], T.R. Junk[8], D. Karlen[6], V. Kartvelishvili[16], K. Kawagoe[24], T. Kawamoto[24], P.I. Kayal[30], R.K. Keeler[28], R.G. Kellogg[17], B.W. Kennedy[20], J. Kirk[29], A. Klier[26], S. Kluth[8], T. Kobayashi[24], M. Kobel[10], D.S. Koetke[6], T.P. Kokott[3], M. Kolrep[10], S. Komamiya[24], T. Kress[11], P. Krieger[6], J. von Krogh[11], P. Kyberd[13], G.D. Lafferty[16], R. Lahmann[17], W.P. Lai[19], D. Lanske[14], J. Lauber[15], S.R. Lautenschlager[31], J.G. Layter[4], D. Lazic[22], A.M. Lee[31], E. Lefebvre[18], D. Lellouch[26], J. Letts[12], L. Levinson[26], S.L. Lloyd[13], F.K. Loebinger[16], G.D. Long[28], M.J. Losty[7], J. Ludwig[10], A. Macchiolo[2], A. Macpherson[30], M. Mannelli[8], S. Marcellini[2], C. Markus[3], A.J. Martin[13], J.P. Martin[18], G. Martinez[17], T. Mashimo[24], P. Mättig[3], W.J. McDonald[30], J. McKenna[29], E.A. Mckigney[15], T.J. McMahon[1], R.A. McPherson[8], F. Meijers[8], S. Menke[3], F.S. Merritt[9], H. Mes[7], J. Meyer[27], A. Michelini[2], G. Mikenberg[26], D.J. Miller[15], A. Mincer[22,e], R. Mir[26], W. Mohr[10], A. Montanari[2], T. Mori[24], M. Morii[24], U. Müller[3], S. Mihara[24], K. Nagai[26], I. Nakamura[24], H.A. Neal[8], B. Nellen[3], R. Nisius[8], S.W. O'Neale[1], F.G. Oakham[7], F. Odorici[2], H.O. Ogren[12], A. Oh[27], N.J. Oldershaw[16], M.J. Oreglia[9], S. Orito[24], J. Pálinkás[33,d], G. Pásztor[32], J.R. Pater[16], G.N. Patrick[20], J. Patt[10], M.J. Pearce[1], R. Perez-Ochoa[8], S. Petzold[27], P. Pfeifenschneider[14], J.E. Pilcher[9], J. Pinfold[30], D.E. Plane[8], P. Poffenberger[28], B. Poli[2], A. Posthaus[3], D.L. Rees[1], D. Rigby[1], S. Robertson[28], S.A. Robins[22], N. Rodning[30], J.M. Roney[28], A. Rooke[15], E. Ros[8], A.M. Rossi[2], P. Routenburg[30], Y. Rozen[22], K. Runge[10], O. Runolfsson[8], U. Ruppel[14], D.R. Rust[12], R. Rylko[25], K. Sachs[10], T. Saeki[24], E.K.G. Sarkisyan[23], C. Sbarra[29], A.D. Schaile[34], O. Schaile[34], F. Scharf[3], P. Scharff-Hansen[8], P. Schenk[34], J. Schieck[11], P. Schleper[11], B. Schmitt[8], S. Schmitt[11], A. Schöning[8], M. Schröder[8], H.C. Schultz-Coulon[10], M. Schumacher[3], C. Schwick[8], W.G. Scott[20], T.G. Shears[16], B.C. Shen[4], C.H. Shepherd-Themistocleous[8],

P. Sherwood[15], G.P. Siroli[2], A. Sittler[27], A. Skillman[15], A. Skuja[17], A.M. Smith[8], G.A. Snow[17], R. Sobie[28], S. Söldner-Rembold[10], R.W. Springer[30], M. Sproston[20], K. Stephens[16], J. Steuerer[27], B. Stockhausen[3], K. Stoll[10], D. Strom[19], P. Szymanski[20], R. Tafirout[18], S.D. Talbot[1], S. Tanaka[24], P. Taras[18], S. Tarem[22], R. Teuscher[8], M. Thiergen[10], M.A. Thomson[8], E. von Törne[3], S. Towers[6], I. Trigger[18], Z. Trócsányi[33], E. Tsur[23], A.S. Turcot[9], M.F. Turner-Watson[8], P. Utzat[11], R. Van Kooten[12], M. Verzocchi[10], P. Vikas[18], E.H. Vokurka[16], H. Voss[3], F. Wäckerle[10], A. Wagner[27], C.P. Ward[5], D.R. Ward[5], P.M. Watkins[1], A.T. Watson[1], N.K. Watson[1], P.S. Wells[8], N. Wermes[3], J.S. White[28], B. Wilkens[10], G.W. Wilson[27], J.A. Wilson[1], G. Wolf[26], T.R. Wyatt[16], S. Yamashita[24], G. Yekutieli[26], V. Zacek[18], D. Zer-Zion[8]

[1]School of Physics and Space Research, University of Birmingham, Birmingham B15 2TT, UK
[2]Dipartimento di Fisica dell' Università di Bologna and INFN, I-40126 Bologna, Italy
[3]Physikalisches Institut, Universität Bonn, D-53115 Bonn, Germany
[4]Department of Physics, University of California, Riverside CA 92521, USA
[5]Cavendish Laboratory, Cambridge CB3 0HE, UK
[6] Ottawa-Carleton Institute for Physics, Department of Physics, Carleton University, Ottawa, Ontario K1S 5B6, Canada
[7]Centre for Research in Particle Physics, Carleton University, Ottawa, Ontario K1S 5B6, Canada
[8]CERN, European Organisation for Particle Physics, CH-1211 Geneva 23, Switzerland
[9]Enrico Fermi Institute and Department of Physics, University of Chicago, Chicago IL 60637, USA
[10]Fakultät für Physik, Albert Ludwigs Universität, D-79104 Freiburg, Germany
[11]Physikalisches Institut, Universität Heidelberg, D-69120 Heidelberg, Germany
[12]Indiana University, Department of Physics, Swain Hall West 117, Bloomington IN 47405, USA
[13]Queen Mary and Westfield College, University of London, London E1 4NS, UK
[14]Technische Hochschule Aachen, III Physikalisches Institut, Sommerfeldstrasse 26-28, D-52056 Aachen, Germany
[15]University College London, London WC1E 6BT, UK
[16]Department of Physics, Schuster Laboratory, The University, Manchester M13 9PL, UK
[17]Department of Physics, University of Maryland, College Park, MD 20742, USA
[18]Laboratoire de Physique Nucléaire, Université de Montréal, Montréal, Quebec H3C 3J7, Canada
[19]University of Oregon, Department of Physics, Eugene OR 97403, USA
[20]Rutherford Appleton Laboratory, Chilton, Didcot, Oxfordshire OX11 0QX, UK
[22]Department of Physics, Technion-Israel Institute of Technology, Haifa 32000, Israel
[23]Department of Physics and Astronomy, Tel Aviv University, Tel Aviv 69978, Israel
[24]International Centre for Elementary Particle Physics and Department of Physics, University of Tokyo, Tokyo 113, and Kobe University, Kobe 657, Japan
[25]Brunel University, Uxbridge, Middlesex UB8 3PH, UK
[26]Particle Physics Department, Weizmann Institute of Science, Rehovot 76100, Israel
[27]Universität Hamburg/DESY, II Institut für Experimental Physik, Notkestrasse 85, D-22607 Hamburg, Germany
[28]University of Victoria, Department of Physics, P O Box 3055, Victoria BC V8W 3P6, Canada
[29]University of British Columbia, Department of Physics, Vancouver BC V6T 1Z1, Canada

[30]University of Alberta, Department of Physics, Edmonton AB T6G 2J1, Canada
[31]Duke University, Dept of Physics, Durham, NC 27708-0305, USA
[32]Research Institute for Particle and Nuclear Physics, H-1525 Budapest, P O Box 49, Hungary
[33]Institute of Nuclear Research, H-4001 Debrecen, P O Box 51, Hungary
[34]Ludwigs-Maximilians-Universität München, Sektion Physik, Am Coulombwall 1, D-85748 Garching, Germany

[a] and at TRIUMF, Vancouver, Canada V6T 2A3
[b] and Royal Society University Research Fellow
[c] and Institute of Nuclear Research, Debrecen, Hungary
[d] and Department of Experimental Physics, Lajos Kossuth University, Debrecen, Hungary
[e] and Department of Physics, New York University, NY 1003, USA

1 Introduction

This paper describes a search for a massive di-photon resonance produced in e^+e^- collisions from $\sqrt{s} = 91$ to 172 GeV. The search presented here is based on a total of 173 pb^{-1} of data taken at $\sqrt{s} \approx 91$ GeV ("LEP1"), 5.4 pb^{-1} taken at $\sqrt{s} = 130 - 140$ GeV ("LEP1.5", also referred to as 133 GeV, which is the luminosity-weighted energy average), and 20.3 pb^{-1} taken at $\sqrt{s} = 161 - 172$ GeV ("LEP2")[1].

For a hypothetical di-photon resonance produced with $M_{\gamma\gamma} > 20$ GeV, the signature is rather distinct from backgrounds because the photons are so energetic. At centre-of-mass energies above the Z^0 the most important background arises from initial state radiation leading to doubly radiative returns to the Z^0 ($e^+e^- \to Z^0(\gamma\gamma)_{\rm ISR}$). The $\gamma\gamma q\bar{q}$, $\gamma\gamma\ell^+\ell^-$, and $\gamma\gamma\nu\bar{\nu}$ final states are a potentially rich hunting ground for non-Standard Model processes. In the case of the Standard Model Higgs boson, $H^0 \to \gamma\gamma$ proceeds by means of a vertex loop and is too small for observation at existing accelerators even for a kinematically accessible Higgs boson [1]. An 80 GeV Higgs boson, for example, has an expected di-photon branching ratio of 1.0×10^{-3}. However, for anomalous Higgs couplings, the production cross section and/or the branching ratio could be large [2]. Of particular interest are so-called Type I Two-Higgs doublet models where one of the doublets couples only to the $SU(2) \times U(1)$ gauge bosons giving rise to a "bosophilic" scalar [3]. Other particles indicative of physics outside the Standard Model might have distinctive signatures in the di-photon decay mode.

There are existing limits on the production of a di-photon resonance which couples to the Z^0 from data taken at $\sqrt{s} \approx 91$ GeV from 1991–1994 [4, 5, 6], and measurements of $\gamma\gamma\nu\bar{\nu}$ at LEP1.5 and at LEP2 have been published [7]. This paper describes the search for a di-photon resonance produced via the process $e^+e^- \to XY$, $X \to \gamma\gamma, Y \to f\bar{f}$ where $f\bar{f}$ may be quarks, charged leptons, or a neutrino pair. For the hadronic final state, no requirement is imposed on the mass recoiling from the di-photon system, hence the search is sensitive to any production of the sort $e^+e^- \to XY$, $X \to \gamma\gamma, Y \to$ hadrons. In order to assess measurements made at different values of $\sqrt{s}$, the data must be analyzed in the context of a production model, therefore the Standard Model and 2-doublet type Higgs models are used in this analysis; in this paper, "H^0" refers to the lightest neutral scalar where doublet models are discussed. Both the LEP1 data and those taken at higher energies contribute significantly to the searches. The larger dataset at LEP1 energies allows for better limits on the cross section for particle masses below approximately 80 GeV, but the final state Z^0 is off mass-shell. The higher energy datasets have lower integrated luminosity, but benefit from the presence of an on-shell Z^0.

2 The OPAL Detector

The OPAL detector is described in detail elsewhere [8]; therefore, only the sub-detectors important for this analysis will be described. The electromagnetic calorimeter (EC) consists of lead-glass blocks of two geometries.

The "barrel" section of the electromagnetic calorimeter covers the polar region $|\cos\theta| < 0.82$, where the polar angle θ was defined with respect to the incident electron beam direction.

[1] More precisely, the LEP1.5 and LEP2 datasets consist of 2.73 pb^{-1} at 130.3 GeV, 2.64 pb^{-1} at 136.2 GeV, 0.05 pb^{-1} at 140.1 GeV, 10.0 pb^{-1} at 161.3 GeV, 1.0 pb^{-1} at 170.3 GeV, and 9.3 pb^{-1} at 172.3 GeV.

In the barrel region, the lead glass calorimeter blocks are 24.6 radiation lengths thick, with each block subtending an angular region of approximately 40×40 mrad^2. The "endcap" sections extends the coverage of the polar region to include $0.81 < |\cos\theta| < 0.98$. In the endcap region, the lead glass calorimeter blocks are approximately 22 radiation lengths thick, with approximately the same angular segmentation as the barrel.

Charged track (CT) reconstruction was achieved using a system of cylindrical tracking detectors contained in a uniform 0.435 T magnetic field. The tracking device central to this analysis was the jet chamber. For the polar angle range $|\cos\theta| < 0.92$, charged tracks are reconstructed with nearly 100% efficiency.

For this analysis, the central jet chamber, endcap and barrel electromagnetic calorimeters were required to be fully operational. The most important detector properties for this analysis were the photon angular and energy resolutions, which yielded a di-photon invariant mass resolution (RMS) approximately equal to $\sigma_{M_{\gamma\gamma}} = 0.42$ GeV $+ 0.02 M_{\gamma\gamma}$, on average, for scalar production in the energy range considered in this paper.

The quality of reconstruction of electromagnetic clusters and the accuracy on the modelling of backgrounds varied in several ranges of the polar angle. The polar angle range $0.82 > |\cos\theta| > 0.81$ is the region of overlap between the barrel and endcap electromagnetic calorimeters; electromagnetic clusters are not as well measured in this region. For $0.8 > |\cos\theta| > 0.7$, material from the jet chamber pressure vessel somewhat degrades photon and electron energy measurement. Inert material in the polar angle range $|\cos\theta| < 0.9$ is well modelled in the Monte Carlo simulation of the OPAL detector; therefore, the polar angle of candidate photons is required to be in this range.

3 Simulation of Signals and Backgrounds

The background sources were modelled by a number of different Monte Carlo simulation programs. The Standard Model backgrounds from $e^+e^- \to (\gamma/Z)^* \to q\bar{q}$ were simulated using the PYTHIA [9] package with the set of hadronization parameters described in reference [10]. Hadronic 4-fermion processes were modelled using the grc4f [11] and EXCALIBUR [12] event generators [2]. The process $e^+e^- \to \gamma\gamma(\gamma)$ was simulated using the RADCOR generator [13]. The programs BHWIDE [14] and TEEGG [15] were utilized to model the background from Bhabha scattering. The processes $e^+e^- \to \ell^+\ell^-$ with $\ell \equiv \mu, \tau$ were simulated using KORALZ [16]. The KORALZ program was also used to generate events of the type $e^+e^- \to \nu\overline{\nu}\gamma(\gamma)$. Four-fermion processes of the type $e^+e^-\ell^+\ell^-$, where $\ell \equiv e, \mu, \tau$, were modelled using the Vermaseren [17] and grc4f generators. The background contributions from the process $e^+e^- \to e^+e^-q\bar{q}$ were simulated using PYTHIA and HERWIG [18].

For the simulation of potential signals, both the HZHA generator [19] and the PYTHIA generator were used to simulate the process of $e^+e^- \to H^0Z^0$ followed by $H^0 \to \gamma\gamma$ for each Z^0 decay channel. For the more general production of scalar/scalar and scalar/vector production, $e^+e^- \to XY \to \gamma\gamma + \textit{hadrons}$, a mass grid was generated. For each X or Higgs mass, production samples of 1000 events were generated from M_X,M_Y = (40,40) GeV, in 20 GeV steps forming an X-Y mass grid, up to the kinematic limit for each of the LEP2 centre-of-mass energies.

[2] The EXCALIBUR and grc4f results were compared within the context of this analysis and found to agree within statistical uncertainty.

For simulation of the 1995 LEP1 data used in this analysis, the JETSET 7.4 [20] and HERWIG 5.8 programs were used. The JETSET program appears to simulate the production of photons and neutral particles better than HERWIG, though both programs underestimate the numbers of low energy isolated photons and π^0 mesons [21].

Both signal and background events were processed using the full OPAL detector simulation [22]. The detector simulation describes the data well except for the low polar angle region mentioned in the previous section.

4 Event Selection

The philosophy adopted in this analysis was to introduce the minimum number of cuts which allow for a relatively uniform acceptance over the largest possible range of masses. The search was divided into three topologies. The first was a search for a system of two photons with large invariant mass recoiling from a hadronic system. The second topology was a search for di-photons produced in association with a Z^0 decaying to charged leptons. The third topology was a search for no significant detector activity other than a di-photon pair. Backgrounds in the cases of the charged lepton and missing energy channels required that the search in these channels be restricted to the case where the di-photon system recoiled from a Z^0 or that the di-photon energies were less that $\sqrt{s}$. However, the exceptionally clean nature of the di-photon final states permitted the use of very loose selection criteria to identify the Z^0 decay products.

Radiative events were distinguished by examining the polar angle distribution of the photons. Photons arising from initial state radiation are close to the beam direction, whereas photons from processes of interest, *i.e.*, $X \to \gamma\gamma$, would be distributed nearly isotropically. The background is serious for photon energies below approximately 10 GeV, corresponding to masses below about 20–30 GeV for the centre-of-mass energies under consideration.

4.1 Photon Identification

Photon candidates were initially selected as "unassociated" electromagnetic calorimeter clusters, where no CT track was reconstructed within the resolution of the EC cluster. To make the photon selection more robust, cuts were made on the lateral spread and isolation of the electromagnetic clusters. Good clusters were required to have lateral sizes consistent with electromagnetic showers. The number of blocks in the cluster ($N_{\rm blk}$) and the number of blocks containing 90% of the cluster energy (N_{90}) were required to be less than some maximum values, depending on the polar angle of the cluster. The barrel and endcap regions of the calorimeter described in Section 2 were treated somewhat differently, and the barrel region was divided into two regions because of differing amounts of inert material in front of the electromagnetic calorimeter in these regions. Clusters containing channels having excessive readout noise were eliminated. The cluster definition cuts were:

- Barrel region I ($|\cos\theta| < 0.7$): $N_{\rm blk} < 15, N_{90} < 3$;
- Barrel region II ($0.7 < |\cos\theta| < 0.81$): $N_{\rm blk} < 25, N_{90} < 4$;
- Barrel-Endcap overlap ($0.81 < |\cos\theta| < 0.82$): $N_{\rm blk} < 35, N_{90} < 5$;

- Endcap ($0.82 < |\cos\theta| < 0.98$): $N_{\rm blk} < 20, N_{90} < 5$.

Photon candidates were then required to satisfy an isolation requirement that rejected events where the electromagnetic cluster energy included particles from the hadronic system. The energy of additional tracks and clusters in a 15° half-angle cone defined by the photon direction had to be less than 2.0 GeV. The distribution of cone energy, after the multiplicity preselection cuts described in the next section, is shown in Figure 1; the distribution of this variable is also shown for the simulated background events. The cone-energy cut reduced the efficiency for signal events by up to 10% due to overlap of the photons with particles from the recoil system. The photon candidates were rejected if there was excessive hadronic energy behind the electromagnetic cluster; hadron calorimeter energy within the photon-defining cone had to be less that 20 GeV. On average, approximately 7% of the photons converted in material in front of the jet chamber, producing tracks in the chamber, and were therefore vetoed in this analysis.

4.2 Hadronic Channel

The hadronic channel consisted of a $\gamma\gamma$ + *hadrons* final state. Candidates for this topology were initially identified by applying a multiplicity preselection consisting of loose charged track multiplicity and visible energy cuts which were used in the standard hadronic event selection described in reference [23]. The preselection cuts were applied to the following measured quantities:

- $E_{\rm cm} \equiv 2 \times E_{\rm beam}$;
- $E_{\rm vis}$: sum of CT track energy, unassociated EC, and unassociated hadron calorimeter clusters;
- $R_{\rm vis} \equiv \frac{E_{\rm vis}}{E_{\rm cm}}$;
- $\vec{p}_{\rm vis}$: vector sum of CT tracks, unassociated EC clusters, and unassociated hadron calorimeter clusters;
- $R_{\rm miss} \equiv \frac{|p_{\rm vis}|}{E_{\rm cm}}$.

The multiplicity preselection cuts required the event to have at least 5 charged tracks and $R_{\rm vis} > 0.1$. Additional "precuts" rejected radiative and $e^+e^-f\bar{f}$ events using the quantities $R_{\rm vis}$ and $R_{\rm miss}$:

- $R_{\rm vis} > 0.6$ and $R_{\rm miss} < (0.5 \times R_{\rm vis} - 0.1)$;
- sum of the visible momentum along the beam direction: $|\Sigma\ p_z^{\rm vis}| < 0.5 \times E_{\rm beam}$;
- event had to have at least 2 electromagnetic clusters with $E > 0.05 \times E_{\rm beam}$.

The distributions of $R_{\rm miss}$ and $R_{\rm vis}$ for simulated signal and backgrounds are shown in Figure 2; the effects of the cuts on data and background simulations are shown in Table 1.

At this point, the background events were almost exclusively from radiative events, predominantly at low energies and large $|\cos\theta|$. Figure 3 shows the distribution for x_γ in data and simulated backgrounds, as well as for a potential Higgs signal, where x_γ is defined as $E_\gamma/E_{\rm beam}$, after applying the multiplicity preselection cuts described in the next section. In the case of simulated signal, the figure indicates cases in which one of the selected EC clusters was not from the correct photon. The incidence of such misidentification falls nearly to zero after more cuts were applied. As indicated in Table 1, there was a dramatic reduction of the backgrounds from all sources simply when two energetic photons were required in the event. An optimal acceptance for the search topology was obtained by imposing cuts on the scaled photon energy:

- Require at least one photon with $x_\gamma > 0.10$, and
- require at least two photons with $x_\gamma > 0.05$.

The key difference between the doubly-radiative photons and those arising from a massive-particle decay is seen in the polar angle distributions of the photons as shown in Figure 4. A cut was therefore imposed to eliminate most of the doubly-radiative events:

- $|\cos\theta_{\gamma 1,2}| < 0.9$ and $|\cos\theta_{\gamma 1}| + |\cos\theta_{\gamma 2}| < 1.4$.

After the cuts on θ_γ, the agreement between data and background simulations (Table 1) was good. Ten events in the LEP1.5 and LEP2 data satisfied all cuts at this point, which can be compared to the Standard Model expectation of 8.3 ± 0.5 events (simulation statistical error). The efficiency for this analysis to accept $\mathrm{H^0Z^0}$ events for $M_{\rm H} = 40$ and 70 GeV is shown in Table 1. Throughout the mass range of interest, an efficiency greater than 45% was maintained.

4.3 Charged Leptonic Channel

The exceptionally clean nature of the $\gamma\gamma\ell^+\ell^-$ final state obviated requiring well-identified leptons. As in the hadronic channel, the most serious background for this channel was doubly radiative returns to the $\mathrm{Z^0}$. Bhabha scattering with initial and/or final state radiation was also a potential background.

Isolated electromagnetic calorimeter clusters and charged tracks satisfying the selection criteria described in reference [24] were used to select charged lepton candidates. To achieve a high efficiency for hadronic τ decays and to ameliorate the possible effects of final state radiation, the selected tracks and clusters were combined into jets using the Durham recombination scheme [25] evaluated with $y_{\rm cut} = 0.02$. Candidates were required to have at least two jets with the possibility of one track defining a jet. The two highest energy electromagnetic clusters satisfying the isolation and cluster quality criteria of Section 4.1 were not included. No distinction between the e, μ and τ channels was made.

Leptonic channel candidates were required to satisfy the following basic selection criteria (referred to as $\ell\ell\gamma\gamma$ preselection):

- Low multiplicity preselection requirements [26];

- precuts particular to the leptonic channel:
  - visible energy fraction: $R_{\rm vis} > 0.2$;
  - number of EC clusters not associated with tracks: $2 \leq N_{\rm EC} \leq 10$;
  - number of good ([24]) charged tracks: $2 \leq N_{\rm CT} \leq 7$;
  - momentum fraction along the beam direction: $|\Sigma\ p_z^{\rm vis}| < 0.7 E_{\rm beam}$.

The following additional criteria were then imposed:

- At least two EC clusters having $|\cos\theta| < 0.966$ and $x_\gamma > 0.1$ satisfying the cluster quality of section 4.1;
- at least two jets found (excluding the photon candidates) within the Durham scheme using $y_{\rm cut} = 0.02$.

To further reduce the background from doubly radiative returns, a likelihood selection based on the photon polar angle distributions was utilized. The relative likelihood of the di-photon system to be consistent with $\mathrm{H}^0 \to \gamma\gamma$ was defined as:

$$\mathcal{L}(\gamma\gamma) = \frac{L(s)}{L(s) + L(b)},$$

where s and b referred to signal and background respectively, and

$$L(x) = \prod_{i=1,2} P(|\cos\theta_{\gamma_i}|), (x = s, b),$$

where $P(|\cos\theta_{\gamma_i}|)$ was the probability of observing photon i at a given $|\cos\theta|$. The reference distributions for the background were taken from $\mathrm{e^+e^-} \to \mathrm{f\bar{f}}\gamma\gamma$ simulations, where $\mathrm{f} \equiv \mu, \tau, \nu$; the electron channel was not used because of the t-channel Bhabha process. For the signal distributions, $\mathrm{H^0Z^0}$ production was assumed with Higgs masses ranging from 30 to 80 GeV. The $|\cos\theta|$ distribution exhibited negligible dependence upon the Higgs mass and $\sqrt{s}$.

Finally, the events had to pass the following two cuts:

- Di-photon likelihood: $\mathcal{L}(\gamma\gamma) > 0.4$;
- recoil mass consistent with the Z^0 mass: $|M_{\rm recoil} - M_{\rm Z}| < 20$ GeV, where the recoil mass was computed as that against the di-photon system.

The cut on the mass recoiling against the di-photon system achieves a rejection factor of at least 2, as seen in Table 2, for a corresponding 5 to 10% loss of acceptance. For events passing the cuts before that on the photon likelihood, the distribution of photon angles is shown in Figure 5. No candidate events were selected at any of the LEP1.5 and LEP2 energies. The contribution from Standard Model processes after the application of all selection criteria was 1.6 ± 0.2, where the error is due to simulation statistics. The analysis is summarized in Table 2, where the expected background from leptonic and $\mathrm{e^+e^-f\bar{f}}$ 4-fermion final states is compared to the observed number of events. The acceptance for $\mathrm{H}^0 \to \gamma\gamma$ ranged from 43–48% for different Higgs masses.

4.4 Missing Energy Channel

The missing energy channel was characterized by a pair of photons recoiling against a massive, unobserved system. The only Standard Model process expected to contribute was doubly radiative return to the Z^0 followed by $Z^0 \to \nu\bar{\nu}$. Potential physics backgrounds included $e^+e^- \to \gamma\gamma(\gamma)$ and radiative Bhabha scattering with one or more unobserved electrons. Backgrounds due to cosmic rays and beam-wall and beam-gas interactions were dealt with as described in reference [27]. Candidates were then required to satisfy in addition the following basic selection criteria (referred to as $\nu\bar{\nu}\gamma\gamma$ preselection):

- 2 electromagnetic clusters with $x_\gamma > 0.1$, satisfying the cluster quality and isolation criteria described in section 4.1;
- $|\Sigma\ p_z^{\rm vis}| < 0.75 E_{\rm beam}$;
- sum of the scaled photon energies: $x_{\gamma 1} + x_{\gamma 2} < 1.4$;
- direction of event missing momentum: $|\cos\theta_{\rm miss}| < 0.96$;
- charged track veto: events were required to have no charged track candidates consistent with originating from the interaction point and having 20 or more jet chamber hits. For tracks at $|\cos\theta| > 0.948$, the requirement on the number of hits was relaxed to 50% of the maximum possible hits, up to a minimum of 10 hits. The distance of closest approach to the interaction point in the plane transverse to the beam direction had to be less than 2 cm and the distance along the beam axis at this point, $|z_0|$, had to be less than 50 cm. To supress backgrounds from beam-gas or beam-wall interactions, events containing one or more tracks with $|z_0| > 50$ cm and having at least 20 jet chamber hits were rejected.
- excess calorimeter energy ($E_{\rm excess}$): the energy observed in the electromagnetic calorimeter not associated with the 2 photons was required to be less than 3 GeV.

At this point the sample was dominated by Bhabha events at small polar angles. The following additional cuts were applied:

- For each photon polar angle: $|\cos\theta| < 0.966$;
- di-photon likelihood: $\mathcal{L}(\gamma\gamma) > 0.4$. The photon candidates were required to pass the likelihood selection described in Section 4.3.

The cut on the sum $x_{\gamma 1} + x_{\gamma 2}$ addresses background from $e^+e^- \to \gamma\gamma$ which gives a peak at $x_{\gamma 1} + x_{\gamma 2} = 2$. A cut on the energy of the di-photon system was found to be more effective than a cut on the acoplanarity angle. Consequently, this channel is only sensitive to di-photon invariant masses up to approximately $0.7\sqrt{s}$.

Three candidates were selected by these cuts in the LEP1.5 and LEP2 data; this is consistent with the Standard Model expectation of 1.8 ± 0.2 events, where the error is due to simulation statistics. The level of the simulated background is dominated by the process $e^+e^- \to \nu\bar{\nu}\gamma\gamma$, which has been estimated using KORALZ [16]. The distribution of recoil mass for these events, prior to the photon likelihood cut, is shown in Figure 6. A summary of the effect of the cuts is given in Table 3 where the efficiencies for Higgs masses of 40 and 70 GeV are also given. The acceptance varied from 42 to 64 % depending on the Higgs mass and centre-of-mass energy.

5 LEP1 Analysis

Earlier searches for the production of a scalar resonance coupling to the Z^0 have been performed using the OPAL detector [4, 5]. For these analyses at $\sqrt{s} \approx 91$ GeV, there is a large background for di-photon invariant masses below approximately 40 GeV. In the hadron channel, a large component of this background arises from radiative photons from the initial and final states, and decays of isolated π^0 and η mesons. The current hadronization simulations JETSET and HERWIG underestimate the rate of this background. Consequently, the LEP1 and LEP2 analyses are compared only for $M_{\gamma\gamma} > 40$ GeV.

In reference [5], $\ell^+\ell^-\gamma\gamma$ ($\ell = \mathrm{e}, \mu, \tau$) and $\nu\bar{\nu}\gamma\gamma$ final states were investigated. From a data sample consisting of 43 pb^{-1}, corresponding to 1.44 million observable Z^0 decays, 2 candidates with $M_{\gamma\gamma} >$ 40 GeV were selected in the $e^+e^-\gamma\gamma$ channel and 2 candidates in the $\mu^+\mu^-\gamma\gamma$ channel. The background expected from the dimuon channel was 1.2 ± 0.3 events.[3]

The hadronic channel was investigated in an earlier publication [4] using LEP1 data from the years 1991 – 1994. A sample of 138 pb^{-1} events was used in this analysis, accumulated at energies between 88.28 and 94.28 GeV, and corresponding to 3.51 million hadronic Z^0 decays. This hadronic channel analysis observed 3 candidates having di-photon mass greater than 40 GeV with an expected background of 5.4 ± 3.0 events. The hadronic channel for an additional 34 pb^{-1} of data was investigated by applying the analysis described in Section 4.2 to LEP1 data from the year 1995, corresponding to 0.72 million hadronic Z^0 decays. To reduce the backgrounds at the LEP1 energy, and to allow for better description of the data by the simulation programs, the cut on photon energies was modified from the one used in Section 4.2:

- $E_{\gamma 1} > 15$ GeV, $E_{\gamma 2} > 15$ GeV.

The hadronic channel 1995 analysis observed one candidate having di-photon mass greater than 40 GeV, at $M_{\gamma\gamma} = 77.2$ GeV. Table 4 shows the events passing the cuts of Section 4.2, as well as the predictions from the simulation programs JETSET 7.4 and HERWIG 5.8. The efficiencies for Higgs boson signals of several masses are also shown in the table.

6 Results

For the higher energy LEP1.5 and LEP2 data, the di-photon invariant mass distribution for the events passing all cuts is shown in Figure 7; the simulation of Standard Model backgrounds is also shown in the figure. Summing over all expected background sources yields 11.7 ± 0.5 events expected versus 13 observed. The kinematic properties of the candidate events are summarized in Table 5. Moreover, the qualitative agreement between the data and simulation of Standard Model processes is good; therefore no new physics process is suggested. After requiring a minimum di-photon mass of 40 GeV, 2 candidates from the LEP1.5 and LEP2 data were left, with the missing-energy and hadronic channels each contributing 1 event; this compares well with the 3.0 ± 0.2 expected from Standard Model backgrounds.

[3] An evaluation of the expected background was only available for the muon channel due to the lack of availability of an event generator for e^+e^- with multiple hard radiated photons at the time of the analysis.

The uncertainties pertinent to the limits on production rates and di-photon branching ratios arose from statistics of the data, systematic uncertainty on the luminosity, statistical errors on background simulations, and a systematic error derived from the level of concordance between backgrounds and their simulation. The systematic error on the integrated luminosity of the data (0.6% for LEP2 energies) contributed negligibly to the limits. Statistical uncertainty on the predicted Standard Model background was dominated by the PYTHIA sample, for which 3000 pb^{-1} was generated at the LEP2 energies. After the cuts on θ_γ and E_γ, which effectively removed the 4-fermion and 2-photon backgrounds, the remaining background was modelled very well by PYTHIA, as demonstrated in Figure 3. The systematic uncertainty on the background modelling was assessed by varying the cuts by one standard deviation on the experimental resolution of the quantity involved. The cuts on photon energies are very robust; uncertainties in electromagnetic cluster energies contribute negligibly to the systematic error. The cut most sensitive to background simulation and detector resolution is that on the photon polar angles. The method of cuts variation gives a possible increase in expected backgrounds smaller that the statistical error on the simulation datasets, approximately 0.2 events in the hadronic channel for the LEP2 data. The same cut-variation technique applied to the efficiency for an expected signal yields a contribution to the systematic uncertainty which is much smaller than the uncertainty from simulation statistics.

From the events passing the cuts, the 95% C.L. upper limit (CLUL) on the number of signal events at a given di-photon mass was computed using the method of Bock [28]. The method introduced for every candidate event a weight based on the di-photon mass resolution and the branching fraction of the Z^0 final state. A mass-dependent 95% confidence level upper limit based on the total weight-sum of all candidate events was computed. The expected backgrounds were not subtracted in computing the 95% CLUL; this results in conservative upper limits. Furthermore, when the statistical method of Bock is used to present the results, where each candidate event weakens the CLUL only in the vicinity of its mass, very little degradation in the upper limits is seen. The results, in the form of upper limits on production cross section (times di-photon branching fraction) are shown in Figure 8; because the energies are similar, the 161 GeV and 172 GeV data have been combined. In computing these limits, the efficiency was set to 0 for recoil masses less than 10 GeV because of uncertainty in simulating the fragmentation process at such low jet energies. The step-like nature of the limit between di-photon masses of 90 and 120 GeV is due to the recoil mass cut in the charged lepton channel and the cut on photon energies in the missing energy channel. The step at 151 GeV is due to the increase in kinematic region afforded by the highest energy (172 GeV) data. The limits from LEP1 are compared to those obtained at LEP2 energies in the figure. The larger LEP1 event sample affords a better limit in the di-photon mass range below 85 GeV. The LEP2 events allow for limits up to nearly twice the LEP1 energy.

To incorporate the $\sqrt{s}$ dependence among the several centre-of-mass energies, the Standard Model $\mathrm{H}^0\mathrm{Z}^0$ production cross section can be factored out of the limits given in Figure 8 to set upper limits on the branching fraction for $\mathrm{H}^0 \to \gamma\gamma$ within the context of this model. This factorization affords a more meaningful presentation of the LEP2 data because of the large phase space factors at $\sqrt{s} = 161 - 172$ GeV (the LEP1.5 data contribute only modestly to these limits because of the lower energy and small integrated luminosity). The resulting limits on $B(\mathrm{H}^0 \to \gamma\gamma)$ are shown in Figure 9, where the limits obtained separately from LEP1, and LEP1.5 and LEP2 combined, are compared. The LEP1 search had one high mass event at $M_{\gamma\gamma} = 77.2$ GeV; this event accounts for the reason the LEP1 data give no useful limit beyond 75 GeV. Figure 9 sets limits on the di-photon branching fraction up to $M_{\mathrm{H}} = 77$ GeV.

The limit on the Standard Model branching ratio shown in Figure 9 can be used to rule out Higgs bosons in certain nonstandard models in which, unlike the minimal Standard Model particle, the Higgs boson couples only to bosons. In the "Bosonic" Higgs model [3], the coupling of the nonstandard Higgs to the Z^0 maintains the Standard Model production rate, while the di-photon branching fraction is larger than 70% for $M_H < 80$ GeV. (In some other models [29] the coupling to the Z^0 is even larger than the minimal Standard Model value.) Using the LEP1, LEP1.5, and LEP2 data, a lower limit of 76.5 GeV is obtained at the 95% confidence level.

More general limits on $e^+e^- \to XY$ production can be obtained using the LEP2 hadronic channel alone. To compute $M_{\gamma\gamma}$ dependent limits, the PYTHIA and HZHA generators have been used to generate a grid of X and Y (recoil particle) masses. It was assumed that X was a scalar, and the cases where Y was a vector or scalar were investigated (the efficiencies were found to be almost equal for Y scalar or vector). Limits were computed using the efficiency at a given $M_{\gamma\gamma}$ which was the minimum for the kinematically allowed variation of M_Y. The limits thus obtained are shown in Figure 10.

7 Conclusions

Using a data sample of 25.7 pb^{-1} taken at centre-of-mass energies from 130 to 172 GeV and 173 pb^{-1} taken near 91 GeV, a search for a massive di-photon resonance has been performed. For $M_{\gamma\gamma} >$ 40 GeV, a total of 2 candidates survived all selection requirements on the LEP1.5 and LEP2 data. The number of observed candidates was consistent with the Standard Model prediction of 3.0 ± 0.2 background events. From the LEP2 data, upper limits on $B(H^0 \to \gamma\gamma) \times \sigma(e^+e^- \to H^0Z^0)$ of 290 – 830 fb are obtained over $40 < M_H < 160$ GeV. From the LEP2 hadronic channel alone, an upper limit on $B(X \to \gamma\gamma) \times B(Y \to hadrons) \times \sigma(e^+e^- \to XY)$, for X a scalar particle, can be placed at 290 fb over the mass range $50 < M_{\gamma\gamma} < 150$ GeV. At $\sqrt{s} \approx 91$ GeV, the LEP1 data upper limit on $B(H^0 \to \gamma\gamma) \times \sigma(e^+e^- \to H^0Z^0)$ is better than 90 fb for $40 < M_{\gamma\gamma} < 80$ GeV. Data from $\sqrt{s} \approx 91$ GeV can be combined with the LEP1.5 and LEP2 data; these combined data can be interpreted within the context of the Standard Model to set a limit on $B(H^0 \to \gamma\gamma)$ up to a Higgs boson mass of 77 GeV, provided the Higgs particle is produced via $e^+e^- \to H^0Z^0$. A lower mass bound of 76.5 GeV is set at the 95% confidence level for Higgs particles which couple only to gauge bosons but still couple to the Z^0 at minimal Standard Model strength.

Acknowledgements

We particularly wish to thank the SL Division for the efficient operation of the LEP accelerator at all energies and for their continuing close cooperation with our experimental group. We thank our colleagues from CEA, DAPNIA/SPP, CE-Saclay for their efforts over the years on the time-of-flight and trigger systems which we continue to use. In addition to the support staff at our own institutions we are pleased to acknowledge the
Department of Energy, USA,
National Science Foundation, USA,
Particle Physics and Astronomy Research Council, UK,
Natural Sciences and Engineering Research Council, Canada,
Israel Science Foundation, administered by the Israel Academy of Science and Humanities,
Minerva Gesellschaft,

Benoziyo Center for High Energy Physics,
Japanese Ministry of Education, Science and Culture (the Monbusho) and a grant under the Monbusho International Science Research Program,
German Israeli Bi-national Science Foundation (GIF),
Bundesministerium für Bildung, Wissenschaft, Forschung und Technologie, Germany,
National Research Council of Canada,
Hungarian Foundation for Scientific Research, OTKA T-016660, T023793 and OTKA F-023259.

References

[1] J. Ellis, M. K. Gaillard, and D. V. Nanopoulos, Nucl. Phys. **B106** (1976) 292.

[2] K. Hagiwara and M.L. Strong, Z. Phys. **C62** (1994) 99.

[3] A. Stange, W. Marciano, and S. Willenbrock, Phys. Rev. **D49** (1994) 1354.

[4] OPAL Collab., G. Alexander *et al.*, Z. Phys. **C71** (1996) 1.

[5] OPAL Collab., P. Acton *et al.*, Phys. Lett. **311** (1993) 391.

[6] L3 Collab., M. Acciarri *et al.*, Phys. Lett. **388** (1996) 409;
DELPHI Collab., P. Abreu *et al.*, Z. Phys. **C72** (1996) 179;
ALEPH Collab., D. Buskulic *et al.*, Phys. Lett. **B313** (1993) 299.

[7] OPAL Collab., G. Alexander *et al.*, Phys. Lett. **B376** (1996) 315;
OPAL Collab., K. Ackerstaff *et al.*, Phys. Lett. **B391** (1997) 210;
ALEPH Collab., D. Buskulic *et al.*, Phys. Lett. **B384** (1996) 333.

[8] OPAL Collab., K. Ahmet *et al.*, Nucl. Instrum. Meth. **A305** (1991) 275;
P.P. Allport *et al.*, Nucl. Instrum. Meth. **A324** (1993) 34;
P.P. Allport *et al.*, Nucl. Instrum. Meth. **A346** (1994) 476;
O.Biebel *et al.*, Nucl. Instrum. Meth. **A323** (1992) 169;
M.Hauschild *et al.*, Nucl. Instrum. Meth. **A314** (1992) 74.

[9] PYTHIA 5.721 and JETSET 7.408 generators:
T. Sjöstrand, Comp. Phys. Comm. **82** (1994) 74;
T. Sjöstrand, LUTP 95-20;
"PYTHIA 5.7 and JETSET 7.4, Physics and Manual", CERN-TH. 7112/93.

[10] OPAL Collab., G. Alexander *et al.*, Z. Phys. **C69** (1996) 543.

[11] J. Fujimoto *et al.*, *GRC4F V1.1: A four fermion event generator for* e^+e^- *collisions*, preprint KEK-CP-046 and e-Print Archive: hep-ph/9605312.

[12] F.A. Berends, R. Pittau and R. Kleiss, Comp. Phys. Comm. **85** (1994) 43.

[13] F.A. Berends and R. Kleiss, Nucl. Phys. **B186** (1981) 22.

[14] S. Jadach, W. Placzek and B. F. L. Ward, University of Tennessee preprint, UTHEP 95-1001 (unpublished).

[15] D. Karlen, Nucl. Phys. **B289** (1987) 23.

[16] S. Jadach et al., Comp. Phys. Comm. **66** (1991) 276.

[17] J. A. M. Vermaseren, Nucl. Phys. **B229** (1983) 347.

[18] G. Marchesini et al., Comp. Phys. Comm. **67** (1992) 465.

[19] HZHA generator: P. Janot, in *Physics at LEP2,* edited by G. Altarelli, T. Sjöstrand and F. Zwirner, CERN 96-01, vol.2 (1996) p.309.

[20] T. Sjöstrand, Comp. Phys. Comm. **39** (1986) 347;
T. Sjöstrand and M. Bengtsson, Comp. Phys. Comm. **43** (1987) 367.

[21] OPAL Collab., G. Alexander *et al.*, Phys. Lett. **B264** (1991) 219.

[22] J.Allison *et al.*, Nucl. Instrum. Meth. **A305** (1992) 47.

[23] OPAL Collab., G. Alexander *et al.*, Z. Phys. **C52** (1991) 175.

[24] OPAL Collab., G. Alexander *et al.*, Z. Phys. **C72** (1996) 191.

[25] N. Brown and W.J. Stirling, Phys. Lett. **B252** (1990) 657;
S. Bethke, Z. Kunszt, D. Soper and W.J. Stirling, Nucl. Phys. **B370** (1992) 310;
S. Catani *et al.*, Phys. Lett. **B269** (1991) 432;
N. Brown and W.J. Stirling, Z. Phys. **C53** (1992) 629.

[26] OPAL Collab., R. Akers *et al.*, Z. Phys. **C61** (1994) 19.

[27] OPAL Collab., R. Akers *et al.*, Z. Phys. **C65** (1995) 47.

[28] P. Bock, *Determination of exclusion limits for particle production using different decay channels with different efficiencies, mass resolutions and backgrounds*, Heidelberg University preprint HD-PY-96/05 (1996); (submitted to Nucl. Instrum. Meth.).

[29] A. G. Akeroyd, Phys. Lett. **B368** (1996) 89.

Cut	Data	ΣBkgd	$(\gamma/Z)^*$	4f	$e^+e^-q\bar{q}$	$M_H = 40$	$M_H = 70$
133 GeV							
Multiplicity	1553	1557.	1529.	16.1	12.0	0.99	0.97
Precuts	736	804.	794.	9.93	0.00	0.91	0.88
$N_\gamma \geq 2$	16	10.4	10.3	0.13	0.00	0.60	0.65
$\cos\theta_\gamma$ cut	6	3.75	3.75	0.00	0.00	0.44	0.51
161 GeV							
Multiplicity	1525	1432.	1346.	55.2	30.6	0.99	0.99
Precuts	523	511.	480.	30.7	0.53	0.87	0.93
$N_\gamma \geq 2$	10	7.95	7.83	0.12	0.00	0.61	0.62
$\cos\theta_\gamma$ cut	3	2.51	2.51	0.00	0.00	0.51	0.49
172 GeV							
Multiplicity	1409	1280.	1126.	126.	28.9	0.99	0.99
Precuts	461	465.	386.	78.5	0.30	0.87	0.92
$N_\gamma \geq 2$	7	6.65	6.64	0.01	0.00	0.67	0.60
$\cos\theta_\gamma$ cut	1	2.00	2.00	0.00	0.00	0.53	0.49

Table 1: Events remaining in the LEP1.5 and LEP2 hadronic channel search after cumulative cuts indicated. The background simulation samples are scaled to 5.4 pb^{-1} for $\sqrt{s} = 133$ GeV, 10.0 pb^{-1} for $\sqrt{s} = 161$ GeV, and to 10.3 pb^{-1} for $\sqrt{s} = 172$ GeV. In addition to the total simulated background, the simulations for $(\gamma/Z)^*$, 4-fermion ("4f"), and Two-photon ($e^+e^-q\bar{q}$) states are shown. "$M_H = 40$" and "$M_H = 70$" indicate the efficiency for simulated H^0Z^0 events with the Higgs mass equal to 40 and 70 GeV, respectively.

Cut	Data	ΣBkgd	e^+e^-	$\tau^+\tau^-$	$\mu^+\mu^-$	e^+e^-ff	$M_H = 40$	$M_H = 70$
135 GeV								
$\ell\ell\gamma\gamma$ presel.	395	179.	55.4	49.6	5.94	68.3	0.78	0.80
$N_\gamma \geq 2$	2	3.96	2.45	0.92	0.56	0.03	0.59	0.61
$N_{\rm jet} \geq 2$	2	2.60	1.36	0.72	0.52	0.01	0.58	0.58
$\mathcal{L}(\gamma\gamma)$	0	1.41	0.65	0.43	0.33	0.01	0.47	0.48
$M_{\rm recoil}$	0	0.68	0.13	0.29	0.25	0.01	0.35	0.04
161 GeV								
$\ell\ell\gamma\gamma$ presel.	434	183.	72.8	46.8	6.73	57.1	0.77	0.81
$N_\gamma \geq 2$	5	5.28	3.44	0.94	0.80	0.10	0.62	0.67
$N_{\rm jet} \geq 2$	1	3.21	1.70	0.67	0.74	0.10	0.60	0.65
$\mathcal{L}(\gamma\gamma)$	0	1.33	0.61	0.33	0.39	0.00	0.49	0.53
$M_{\rm recoil}$	0	0.60	0.24	0.15	0.21	0.00	0.46	0.48
172 GeV								
$\ell\ell\gamma\gamma$ presel.	323	173.	67.8	39.9	5.80	59.1	0.77	0.80
$N_\gamma \geq 2$	5	4.70	2.74	0.83	0.69	0.43	0.61	0.60
$N_{\rm jet} \geq 2$	1	2.65	1.08	0.61	0.63	0.33	0.58	0.58
$\mathcal{L}(\gamma\gamma)$	0	1.17	0.42	0.32	0.32	0.10	0.49	0.47
$M_{\rm recoil}$	0	0.36	0.08	0.14	0.15	0.00	0.43	0.45

Table 2: Events remaining after cumulative cuts indicated, for the LEP1.5 and LEP2 leptonic channel analysis. The row denoted "$\ell\ell\gamma\gamma$ presel." refers to the combined general low-multiplicity selection and the precuts described in Section 4.3. The contributions from e^+e^--pair, μ-pair, τ-pair production and $e^+e^-f\bar{f}$ final states determined from background simulations are shown. The simulated datasets have been normalized to 5.4 pb^{-1} for $\sqrt{s}$ = 133 GeV, 10.0 pb^{-1} for $\sqrt{s}$ = 161 GeV, and to 10.3 pb^{-1} for $\sqrt{s}$ = 172 GeV. Also shown is the acceptance for a Higgs signal for 40 and 70 GeV mass denoted as columns "$M_H = 40$" and "$M_H = 70$", respectively. The poor agreement between data and background simulations in the preselection category results from inadequate modelling of material near the beampipe in the forward region.

Cut	Data	ΣBkgd	e^+e^-	$\nu\bar{\nu}\gamma\gamma$	$\gamma\gamma$	$\ell^+\ell^-$	e^+e^-ff	$M_H = 40$	$M_H = 70$
133 GeV									
$\nu\bar{\nu}\gamma\gamma$ presel.	32	1.73	0.19	0.74	0.80	0.01	0.00	0.68	0.64
$\theta_{\gamma 1}$	4	1.26	0.06	0.74	0.45	0.01	0.00	0.67	0.63
$\theta_{\gamma 2}$	2	0.90	0.06	0.74	0.10	0.01	0.00	0.67	0.63
$\mathcal{L}(\gamma\gamma)$	0	0.59	0.00	0.54	0.05	0.00	0.00	0.58	0.55
161 GeV									
$\nu\bar{\nu}\gamma\gamma$ presel.	32	8.02	5.49	0.98	1.30	0.04	0.21	0.65	0.70
$\theta_{\gamma 1}$	5	4.85	3.21	0.98	0.64	0.02	0.00	0.64	0.70
$\theta_{\gamma 2}$	1	2.01	0.73	0.98	0.29	0.01	0.00	0.63	0.69
$\mathcal{L}(\gamma\gamma)$	1	0.63	0.00	0.55	0.08	0.00	0.00	0.54	0.58
172 GeV									
$\nu\bar{\nu}\gamma\gamma$ presel.	27	7.88	4.83	0.93	1.15	0.03	0.93	0.62	0.72
$\theta_{\gamma 1}$	5	4.54	2.80	0.93	0.59	0.01	0.21	0.61	0.72
$\theta_{\gamma 2}$	3	1.48	0.32	0.93	0.23	0.01	0.00	0.60	0.71
$\mathcal{L}(\gamma\gamma)$	2	0.54	0.00	0.44	0.10	0.00	0.00	0.53	0.62

Table 3: Events remaining after cumulative cuts indicated for the LEP1.5 and LEP2 missing energy channel search. The row denoted "$\nu\bar{\nu}\gamma\gamma$ presel." refers to the combined general low-multiplicity selection and the precuts described in Section 4.4. The contributions from e^+e^--pair, $\nu\bar{\nu}\gamma\gamma$, $\gamma\gamma$, lepton pair ($\ell \equiv \mu, \tau$) production and $e^+e^-f\bar{f}$ final states determined from background simulations are shown. The simulation datasets have been normalized to 5.4 pb^{-1} for $\sqrt{s} = 133$ GeV, 10.0 pb^{-1} for $\sqrt{s} = 161$ GeV, and to 10.3 pb^{-1} for $\sqrt{s} = 172$ GeV. Also shown is the acceptance for a Higgs signal for 40 and 70 GeV mass denoted as columns "$M_H = 40$" and "$M_H = 70$", respectively. The poor agreement between data and background simulations in the preselection category results from inadequate modelling of material near the beampipe in the forward region.

Cut	Data	JETSET 7.4	HERWIG 5.8	$M_H = 40$	$M_H = 70$
Multiplicity	720432	720432	720432	0.99	0.91
Precuts	469235	471123.	465251	0.94	0.85
$N_\gamma \geq 2$	13	5.13	4.00	0.50	0.61
$\cos\theta_\gamma$ cut	2	3.67	2.00	0.38	0.45

Table 4: Events remaining in the 1995 LEP1 hadronic channel search after cumulative cuts indicated. The background predictions for the JETSET 7.4 and HERWIG 5.8 $(\gamma/Z)^*$ simulations are shown; the simulations have been scaled to the number of multihadrons in the data passing the multiplicity cut. "$M_H = 40$" and "$M_H = 70$" indicate the efficiency for simulation of H^0Z^0 events with the Higgs mass equal to 40 and 70 GeV, respectively. The poor agreement between data and simulations at the $N_\gamma \geq 2$ cut is due to poor modelling of isolated π^0 mesons.

Channel	$\sqrt{s}$(GeV)	$M_{\gamma\gamma}$(GeV)	M_{recoil} (GeV)	$\mathrm{E}_{\gamma 1}$ (GeV)	$\cos\theta_{\gamma 1}$	$\mathrm{E}_{\gamma 2}$ (GeV)	$\cos\theta_{\gamma 2}$
$\nu\bar{\nu}$	172	44.9 ± 1.2	93.1	48.7	0.90	18.0	-0.27
$\mathrm{q\bar{q}}$	161	42.2 ± 1.8	79.9	39.2	-0.04	27.0	-0.81
$\nu\bar{\nu}$	172	39.9 ± 3.0	92.6	51.1	0.05	14.7	0.79
$\mathrm{q\bar{q}}$	172	36.8 ± 1.4	90.4	60.3	0.63	5.8	-0.31
$\mathrm{q\bar{q}}$	130	31.0 ± 1.5	89.4	23.7	-0.35	14.4	10.71
$\mathrm{q\bar{q}}$	130	28.7 ± 1.0	91.7	24.9	0.51	11.2	0.51
$\mathrm{q\bar{q}}$	130	25.9 ± 1.1	86.0	31.0	0.57	8.3	0.61
$\mathrm{q\bar{q}}$	161	24.9 ± 1.0	72.1	54.5	0.66	11.8	0.63
$\mathrm{q\bar{q}}$	136	22.5 ± 1.0	82.0	40.7	0.64	4.6	0.42
$\nu\bar{\nu}$	161	15.8 ± 0.5	106.9	32.4	0.58	13.4	0.10
$\mathrm{q\bar{q}}$	136	13.5 ± 1.1	109.7	19.6	-0.74	5.1	0.36
$\mathrm{q\bar{q}}$	161	12.1 ± 0.5	85.6	53.1	0.60	5.1	-0.10
$\mathrm{q\bar{q}}$	130	6.4 ± 0.2	63.4	34.1	-0.47	15.8	-0.21

Table 5: Masses and energies of candidate events from the LEP1.5 and LEP2 searches, after all cuts except the one on di-photon mass. The events are ordered by di-photon mass.

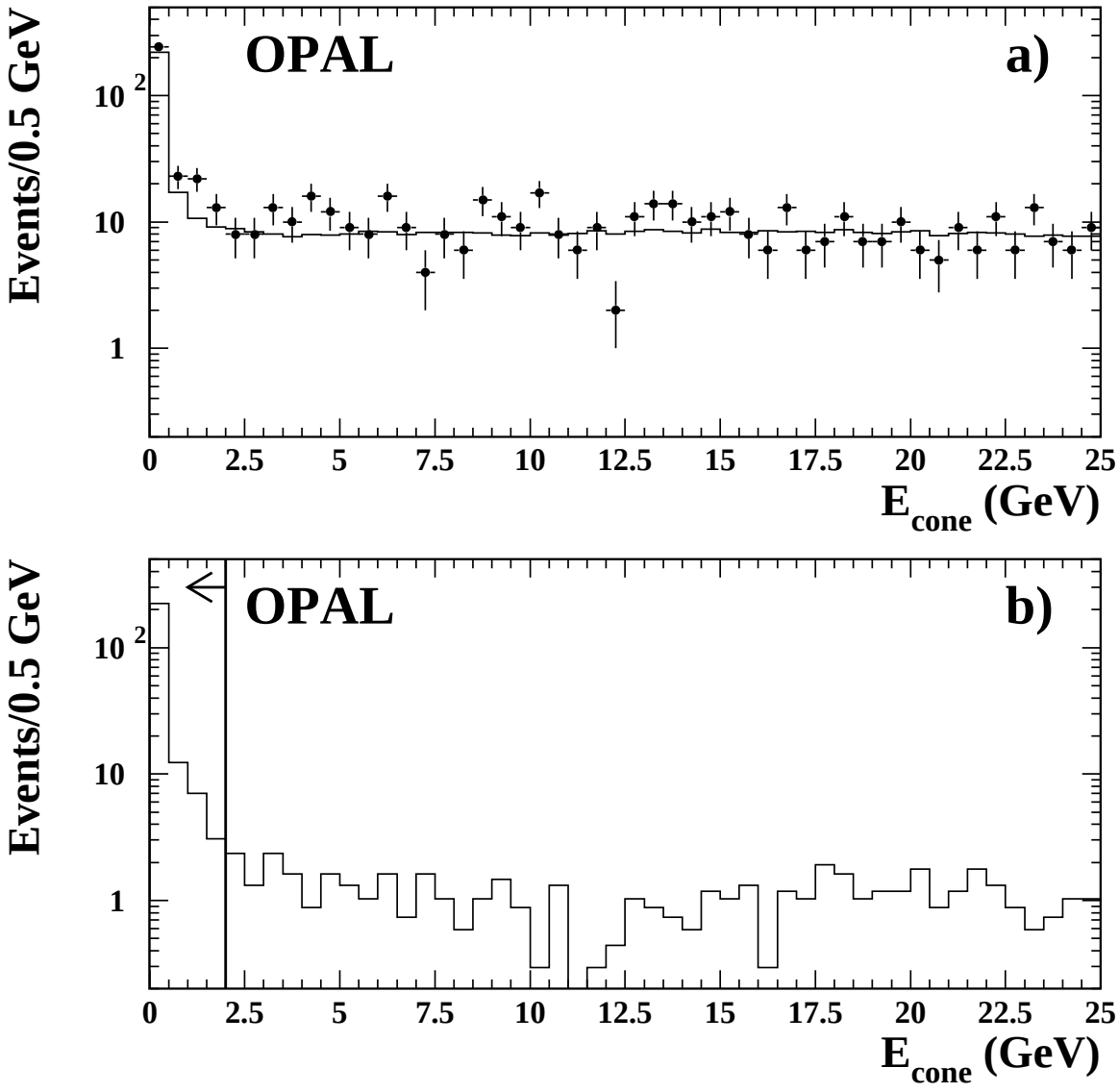

Figure 1: Distribution of charged-particle momentum and unassociated electromagnetic energy sum in 15° cones about the photon axes (for the hadron channel after multiplicity preselection). (a) 161 GeV data (points) and simulated background (histogram). (b) HZ production with $M_{\mathrm{H}} = 40$ GeV. The position of the cut is shown.

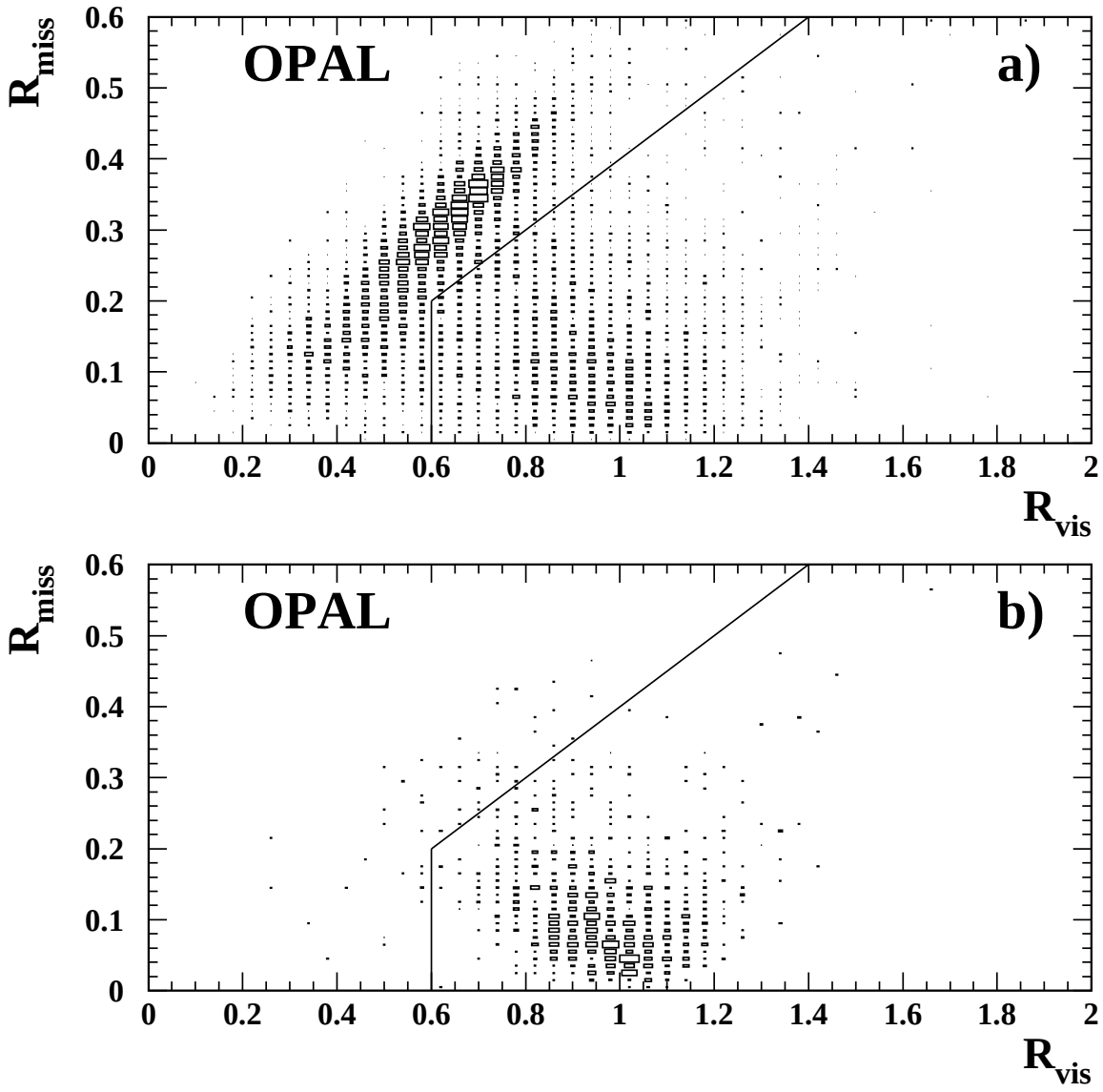

Figure 2: Distribution of fractional visible total energy versus fractional missing momentum for (a) simulation of $q\bar{q}$ events at $\sqrt{s} = 161$ GeV, and (b) simulation of Higgs events with $M_H = 40$ GeV. The cut used for the hadronic channel is shown by the solid line.

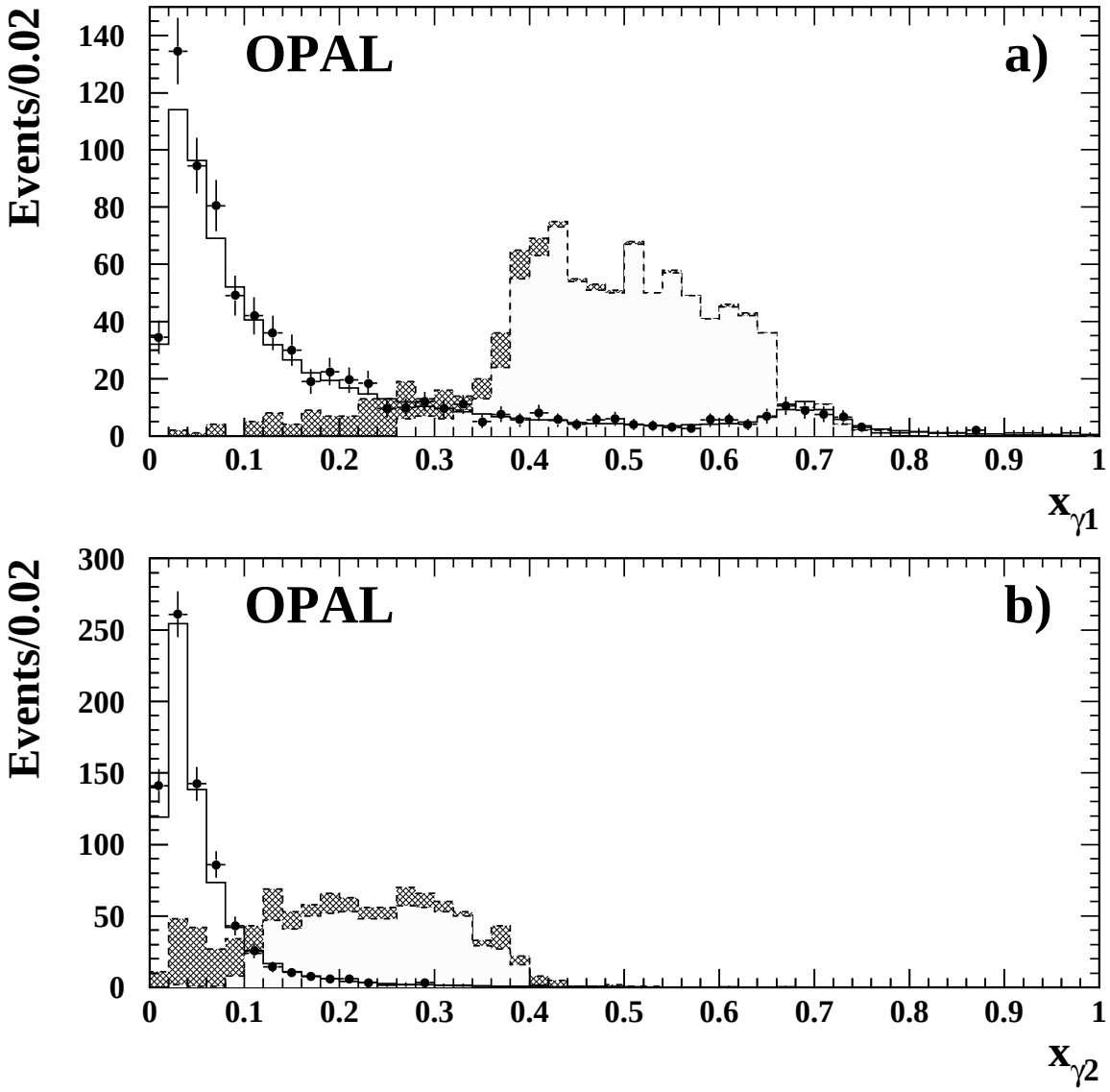

Figure 3: Distribution of $x_\gamma \equiv E_\gamma / E_{\rm beam}$ for the most energetic photon (a) and the second-most energetic photon (b) in the ($\gamma\gamma$ + *hadrons*) search, after the multiplicity preselection. Data from $\sqrt{s} = 161$ GeV are shown as points with error bars; background simulation is indicated by the histogram. The broken histogram shows H^0Z^0 production with $M_{\rm H} = 40$ GeV. The hatched histogram shows simulation cases where the selected electromagnetic cluster was not due to the photon from the Higgs boson.

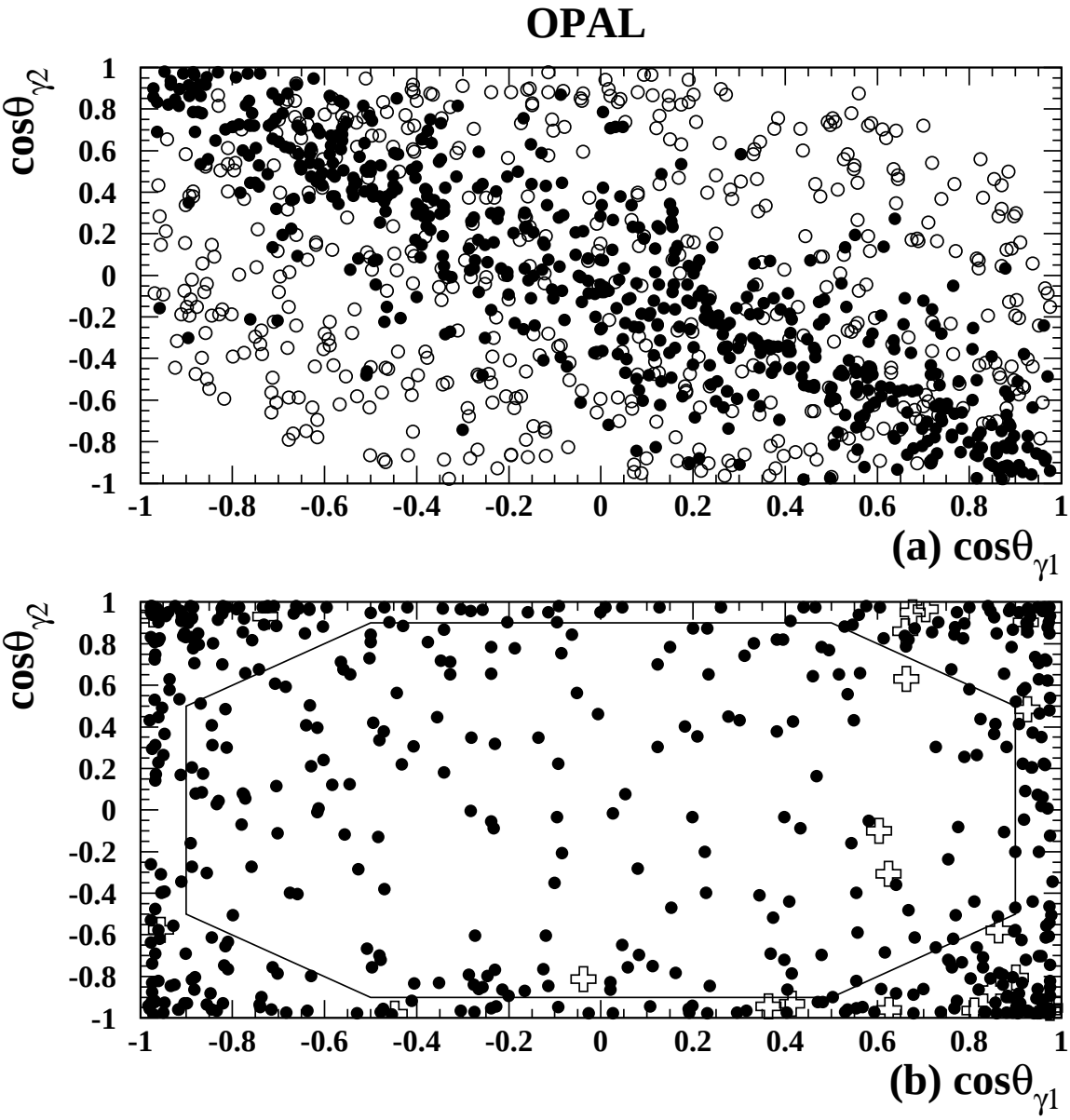

Figure 4: Distribution of $\cos\theta_{\gamma 1}$ and $\cos\theta_{\gamma 2}$ for simulation events of H^0Z^0 production at $\sqrt{s} =$ 161 GeV in the hadronic search channel; the precuts have been applied. (a) shows simulated signal for $M_H = 40$ GeV (open circles) and $M_H = 70$ GeV (solid dots). (b) shows simulated $q\bar{q}$ events and the graphical cut boundary used in the hadronic channel. The data ($\sqrt{s} = 161$ and 172 GeV) are shown as open crosses.

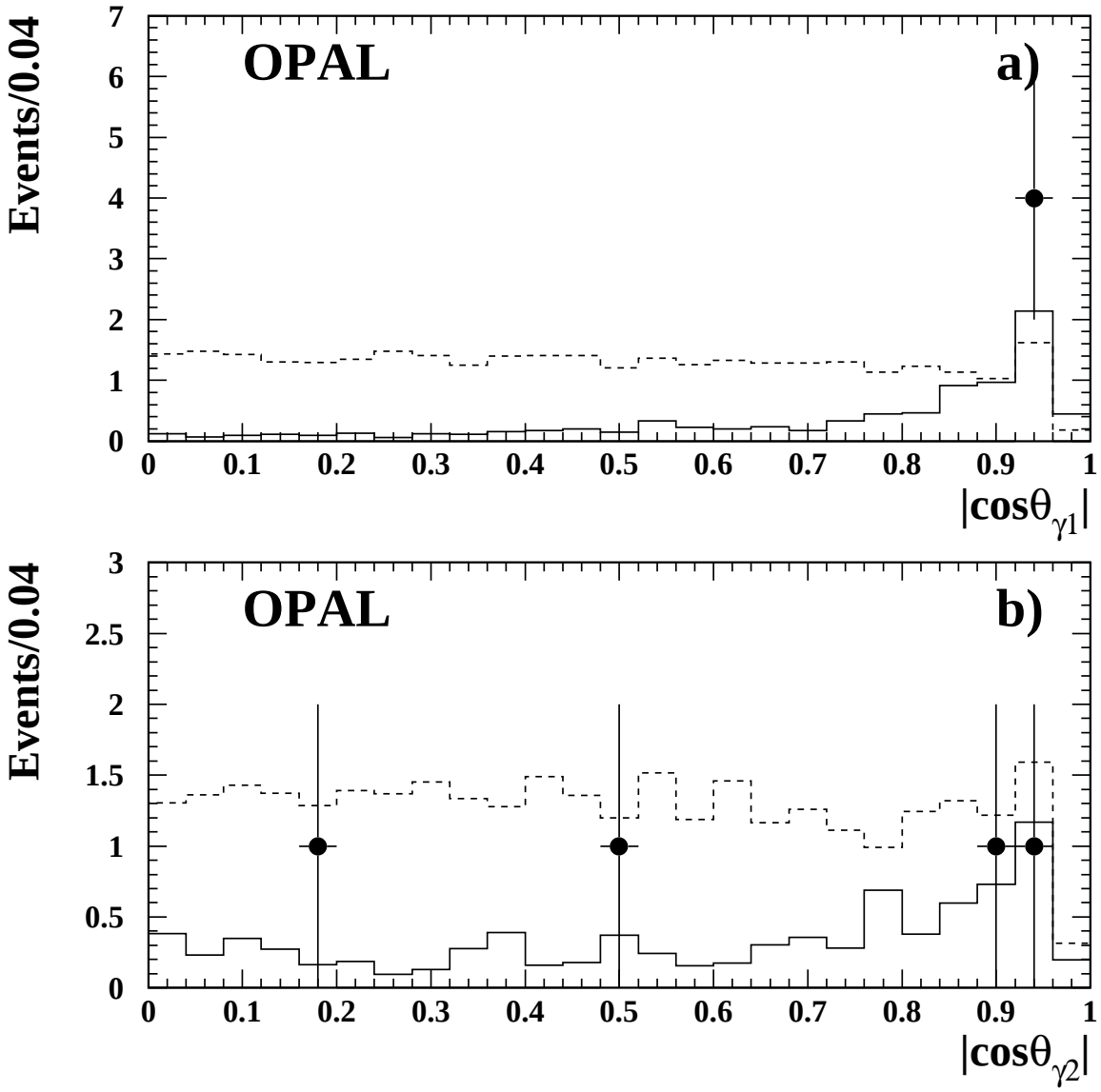

Figure 5: Distribution of photon polar angles for lepton channel LEP1.5 and LEP2 event candidates, before the likelihood cut. The highest energy photon is shown in a); the lower energy photon is shown in b). Background simulation is indicated by the solid histogram. The distribution for a 70 GeV Higgs boson is indicated by the broken histogram.

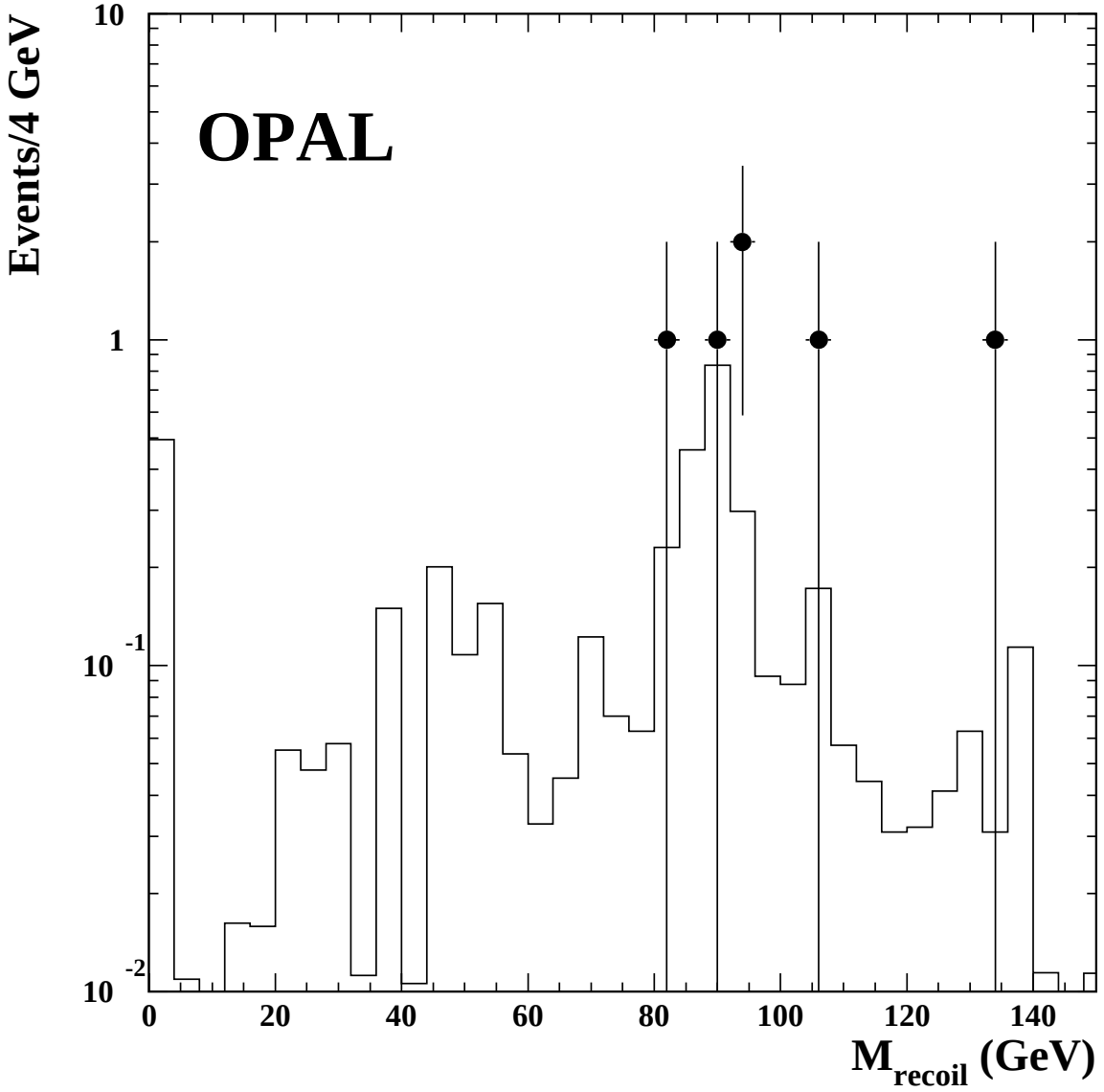

Figure 6: Recoil mass for missing energy channel LEP1.5 and LEP2 event candidates, before the cut on likelihood. Background simulation is indicated by the solid histogram.

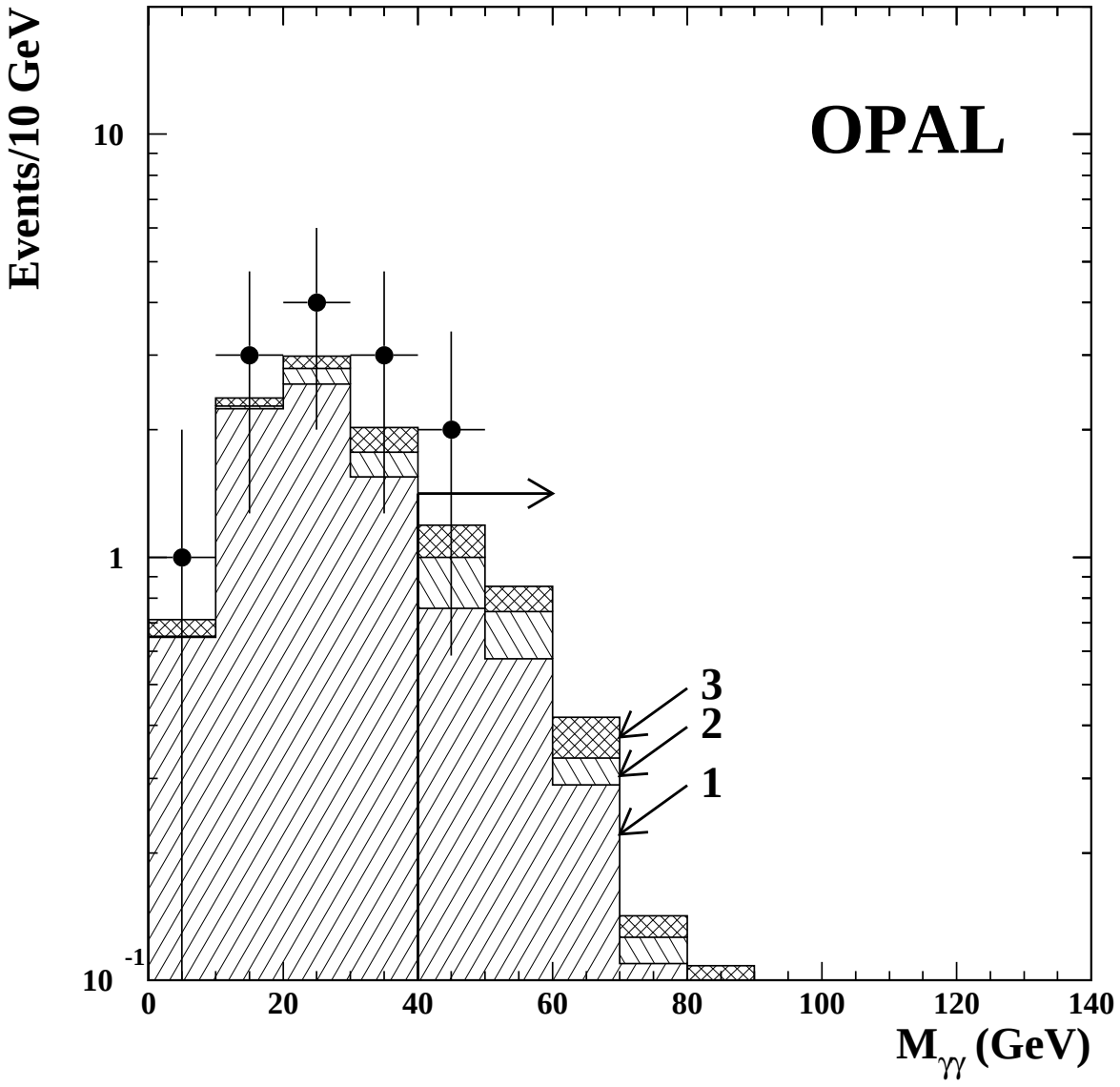

Figure 7: Distribution of mass of the two highest energy photons for LEP1.5 and LEP2 events, after all cuts except the one on $M_{\gamma\gamma}$; all search channels are included. Data are shown as points with error bars. Background simulation is shown as a histogram with (1) indicating the hadronic search channel, (2) indicating the charged lepton search channel, and (3) indicating the missing energy search channel. The $M_{\gamma\gamma}$ cut is indicated.

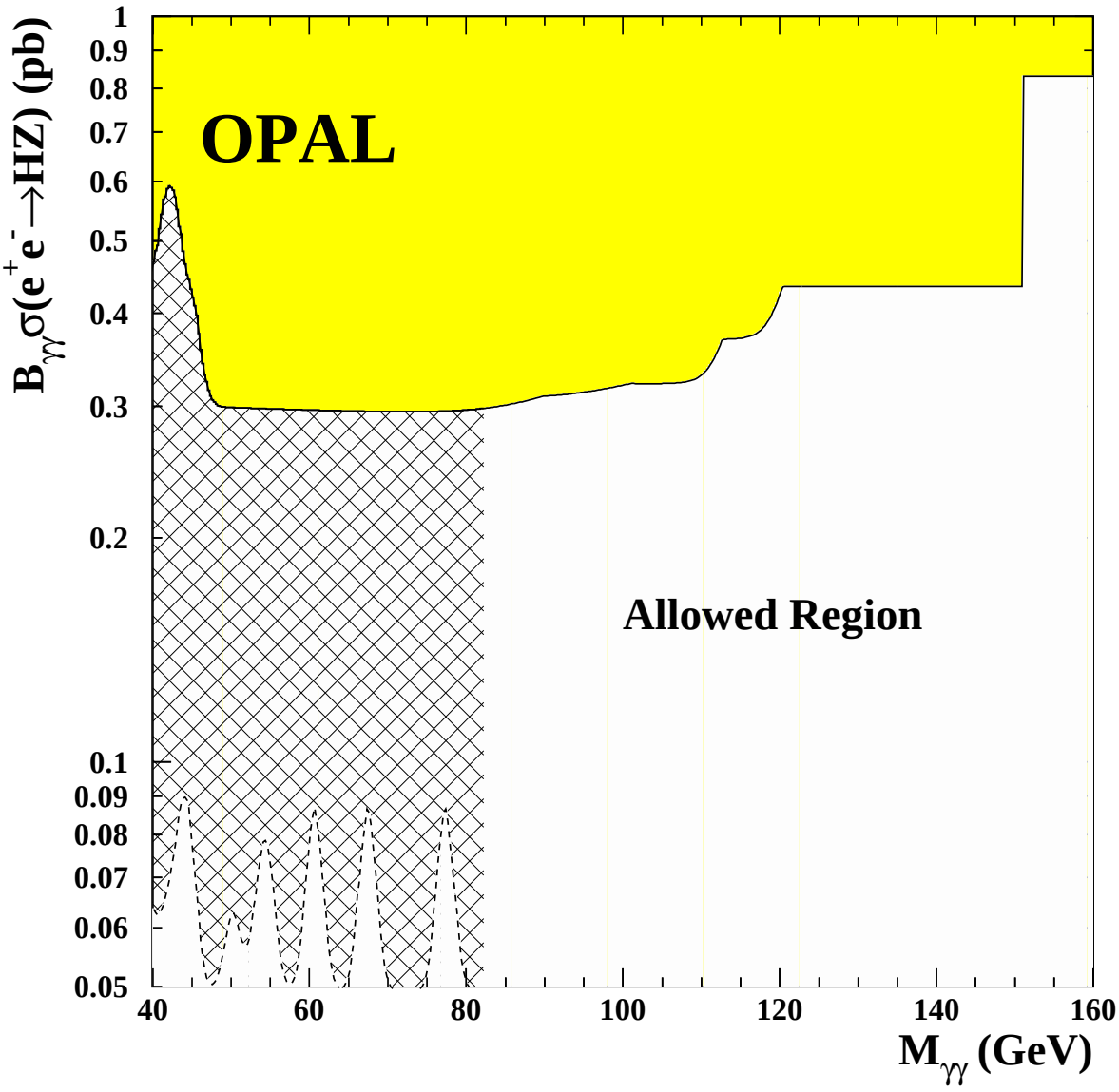

Figure 8: 95% Confidence Level Upper Limit on $B(\mathrm{H}^0 \to \gamma\gamma) \times \sigma(\mathrm{e}^+\mathrm{e}^- \to \mathrm{H}^0\mathrm{Z}^0)$. Solid curve represents the LEP2 limit for $\sqrt{s} = 161 - 172$ GeV; the shaded region is excluded. The cross-hatched region is excluded by the LEP1 analysis for $\sqrt{s} \approx 91$ GeV.

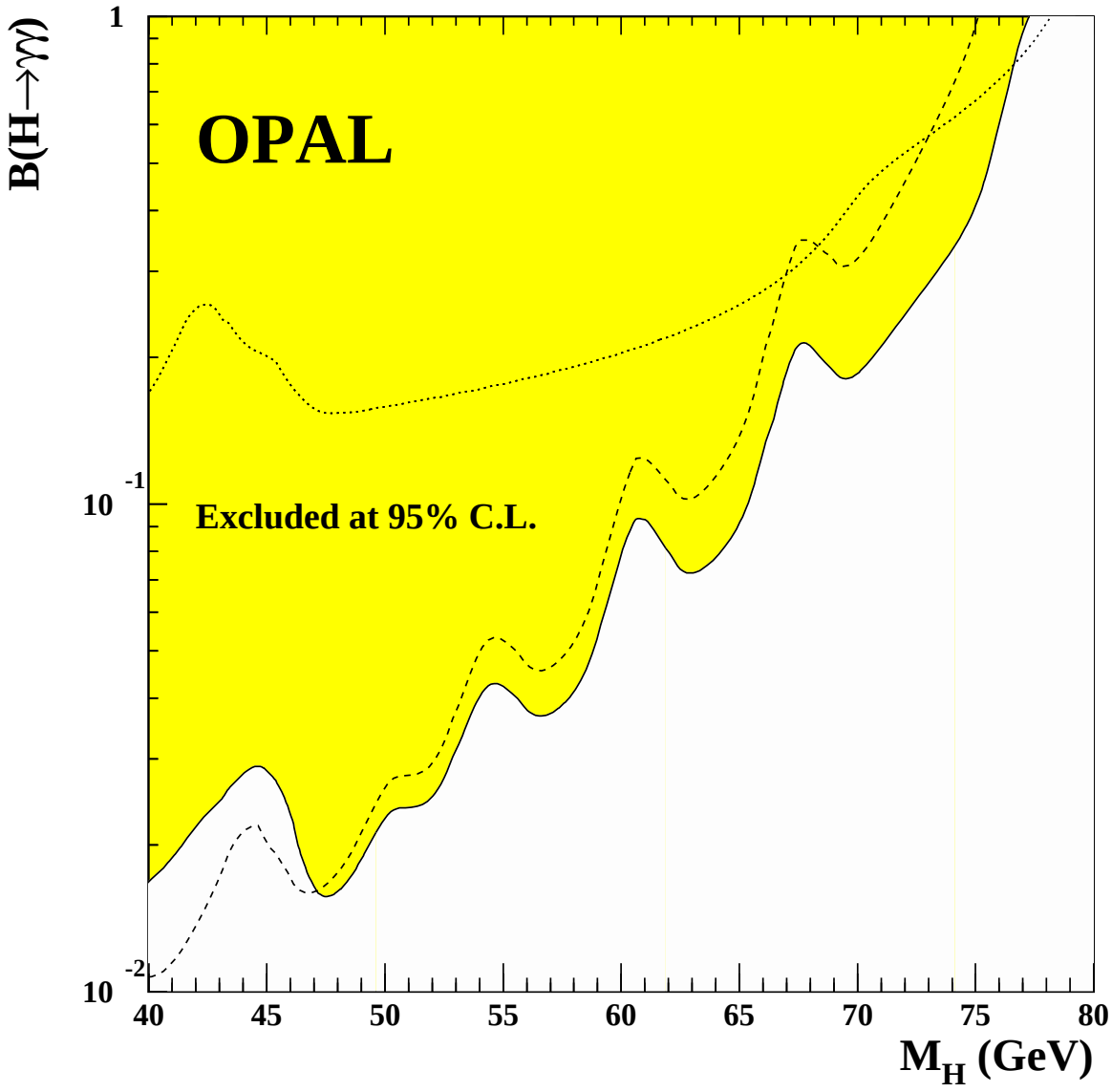

Figure 9: 95% Confidence Level Upper Limit on $B(\mathrm{H}^0 \to \gamma\gamma)$ for Standard Model Higgs boson production using data from $\sqrt{s} = 91$ GeV (dashed line), 133, 161 and 172 GeV (dotted line), and all data combined (solid line). The shaded region is excluded.

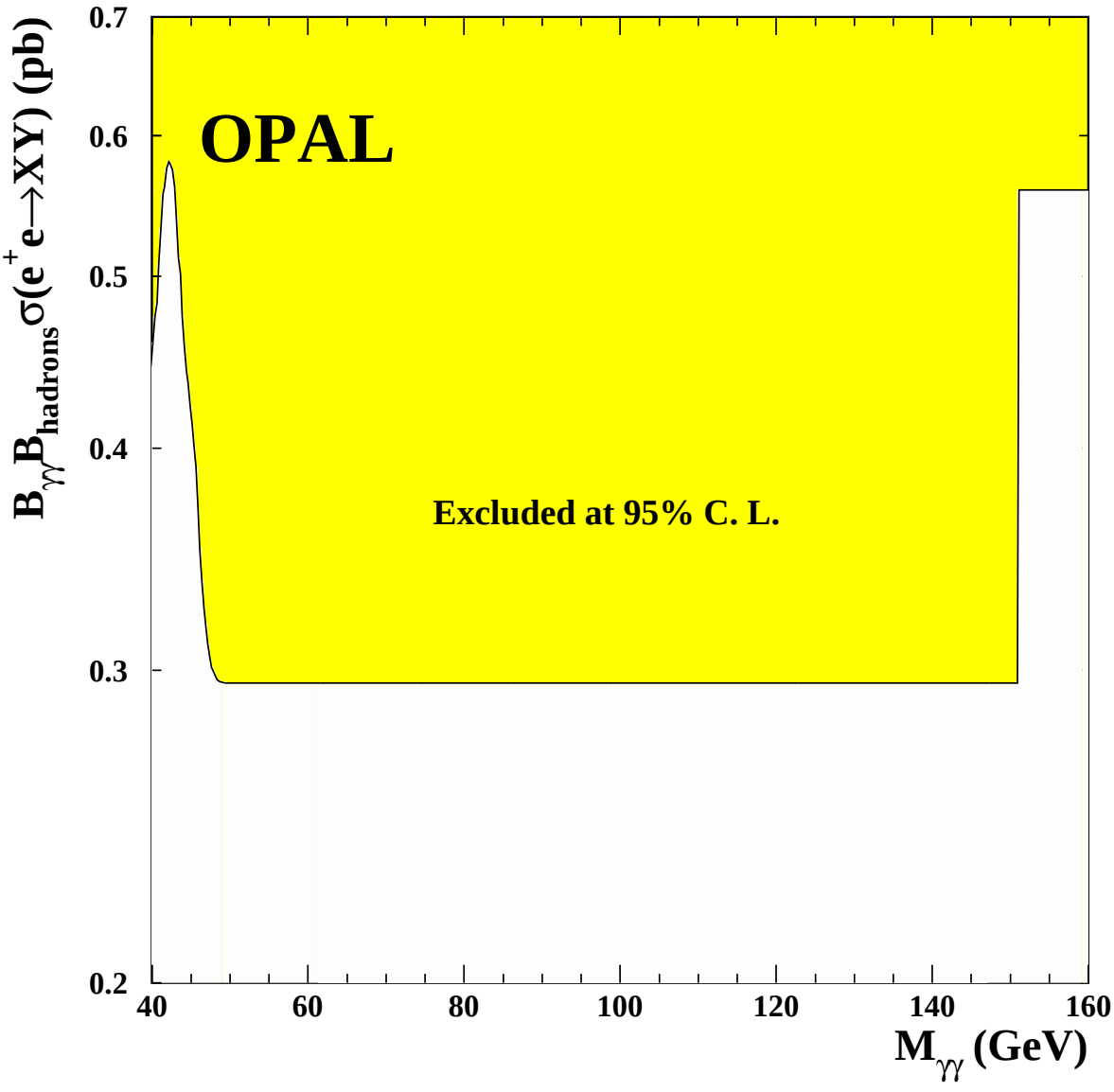

Figure 10: 95% Confidence Level Upper Limit on $B(\mathrm{X} \to \gamma\gamma) \times B(\mathrm{Y} \to hadrons) \times \sigma(\mathrm{e^+e^-} \to \mathrm{XY})$, for scalar X and vector Y, using the hadronic channel analysis with data from LEP2. The shaded region is excluded.